Energy Storage

International Edition: DOI: 10.1002/anie.201700686
German Edition: DOI: 10.1002/ange.201700686

Strings of Porous Carbon Polyhedrons as Self-Standing Cathode Host for High-Energy-Density Lithium–Sulfur Batteries

Yazhi Liu[+], Gaoran Li[+], Jing Fu, Zhongwei Chen, and Xinsheng Peng**

Abstract: *Rational design of cathode hosts with high electrical conductivity and strong sulfur confinement is a great need for high-performance lithium–sulfur batteries. Herein, we report a self-standing, hybrid-nanostructured cathode host comprised of metal–organic framework (MOF)-derived porous carbon polyhedrons and carbon nanotubes (CNTs) for the significant improvement of both the electrode cyclability and energy density. The strong coupling of the intertwined CNTs and strung porous carbon polyhedrons as a binder-free thin film significantly enhances the long-range electronic conductivity and provides abundant active interfaces as well as robust electrode integrity for sulfur electrochemistry. Attributed to the synergistic combination of the CNTs and carbon polyhedrons, the obtained sulfur electrodes exhibit outstanding cyclability, an excellent high-rate response up to 10 C, and an ultra-high volumetric capacity of 960 Ah L^{-1}.*

Lithium–sulfur (Li–S) batteries, holding intrinsic merits such as high energy density, low cost, and environmental friendliness, have emerged as one of the most promising candidates for the next-generation battery system.[1–3] Nevertheless, several issues must be addressed in promoting their practical applications, namely, the poor electronic and ionic conductivity of sulfur and its lithiation products, the high dissolution and the parasitic shuttling behavior of the intermediate polysulfides, and the large volume change (ca. 76%) during the charge–discharge process.[4–7]

Improving the sulfur electrochemistry by means of the advanced cathode material design is a grand challenge that must be solved to make Li–S batteries commercially viable.[8–12] Carbon-based materials have been developed as the most promising sulfur host to address these problems by offering favorable electronic conductivity and effective sulfur confinement,[13–16] among which the metal–organic framework (MOF)-derived porous carbon materials have been recently intensively studied.[17–19] The MOF materials serve as both carbon precursor and template to produce high porosity, which offers abundant electrode/electrolyte interfaces for fast sulfur electrochemistry and uniform sulfur/lithium sulfide deposition. However, because of the powdery MOF-derived carbon, the electron transfer within the bulk electrode is significantly limited owing to the poor contact between powder particles, let alone the further conductivity degradation caused by the use of nonconductive polymer binder.[20,21] In contrast, carbon nanotubes (CNTs), which have highly extended one-dimensional graphitic structures, are capable of offering favorable long-range conductivity within the electrode.[22–24] Additionally, the excellent mechanical properties of CNTs also favor the fabrication of self-standing and flexible electrodes to accommodate the volume change during cycling and allows to simultaneously avoid the employment of nonconductive polymer binder. Nevertheless, the lack of porosity of CNTs fails to provide sufficient active interfaces for full sulfur electrochemistry.

Herein, we present a novel interpenetrated and self-standing conductive framework (ISCF) by the coupling of intertwined CNTs and strung MOF-derived porous carbon polyhedrons to obtain a desirable improvement of sulfur electrochemistry and energy density for Li–S batteries. In such cathode construction, the CNTs penetrate throughout the MOF (that is, $Cu_3(BTC)_2$, HKUST-1)-derived porous carbon polyhedrons and intertwines with the external CNT network, thus weaving the electrode into a robust self-standing and flexible thin film. This hybrid electrode design is endowed with multiple structural advantages: 1) The highly porous carbon polyhedrons ensure a uniform sulfur distribution, strong sulfur confinement, and abundant electrode/electrolyte interfaces for fast electron/ion transfer; 2) the CNT penetration enriches the inner space of the carbon polyhedrons to provide more active interfaces for more thorough sulfur electrochemistry inside the pores; 3) the intertwined CNT network boosts the interfacial contact between polyhedrons and offers significant long-range conductivity, which is particularly intriguing to the high sulfur loading; and 4) the self-standing electrode design, devoid of polymer binders, further improves the conductivity of the cathode, as well as offering a good accommodation against the volume variation during the cycling. Benefiting from these favorable effects, the resultant sulfur electrodes achieved excellent cyclability over 500 cycles at 1 C, outstanding rate capability at up to 10 C, high areal capacity of 6.23 mAh cm^{-2}, and an ultra-high volumetric capacity of 960 Ah L^{-1}.

Scheme 1 shows the typical synthesis of the S@ISCF composite film (for experimental details, see the Supporting Information). Attributed to the electrostatic attraction, the positively charged copper hydroxide nanostrands (CHN) and pre-treated negatively charged CNTs are uniformly inter-

[*] Y. Liu,[+] Prof. X. Peng
Key Laboratory of Silicon Materials, School of Materials Science and Engineering, Zhejiang University
38 Zheda Rd, Hangzhou 310027 (China)
E-mail: pengxinsheng@zju.edu.cn
Dr. G. Li,[+] J. Fu, Prof. Z. Chen
Department of Chemical Engineering, University of Waterloo
200 University Avenue West, Waterloo, Ontario, N2L 3G1 (Canada)
E-mail: zhwchen@uwaterloo.ca
[+] These authors contributed equally to this work.
Supporting information and the ORCID identification number(s) for the author(s) of this article can be found under: http://dx.doi.org/10.1002/anie.201700686.

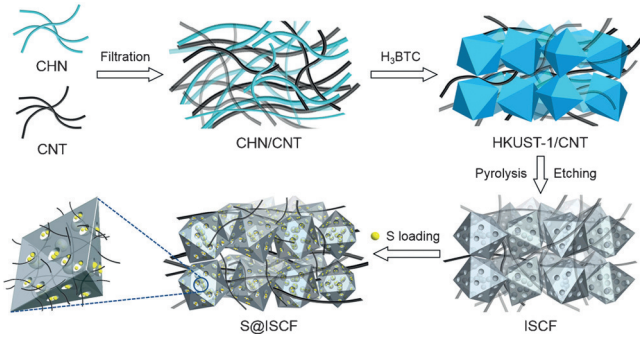

Scheme 1. Schematic of the fabrication process of a S@ISCF composite film.

woven and filtrated into a self-standing hybrid thin film (CHN/CNT, as shown in Supporting Information, Figure S1 a,b).[25] The obtained CHN/CNT thin film exhibits a thickness of 4.3 μm. The CHN/CNT thin film transforms into a HKUST-1/CNT hybrid thin film after immersion in a 1,3,5-benzenetricarboxylic acid (H_3BTC) solution for 1 h, which is confirmed by the XRD patterns (Figure S1 c).[26] The as-developed HKUST-1/CNT hybrid thin film has a HKUST-1/CNT weight ratio of circa 10:1 and a thickness of around 20 μm with a laminated structure constructed by interwoven CNTs and octahedral HKUST-1 crystals (Figure 1 a,b).

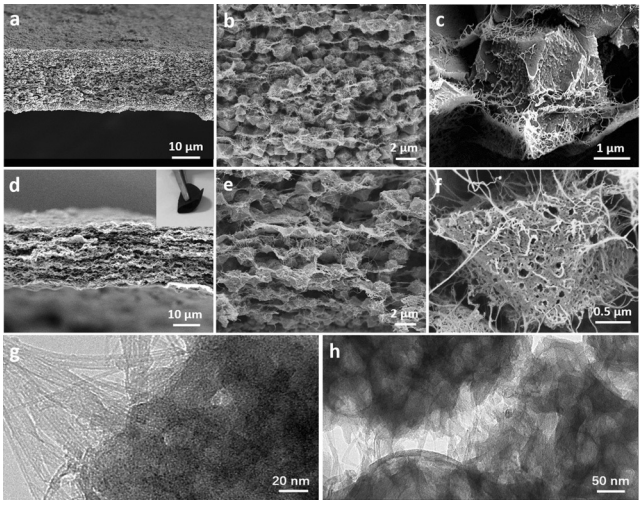

Figure 1. SEM images of a,b) HKUST-1/CNT thin film and c) a fractured crystal in HKUST-1/CNT film. d,e,f) SEM images and g,h) TEM image of ISCF film. The inset in (d) shows the flexibility of the as-prepared ISCF film.

Owing to the uniform interweavement in the CHN/CNT precursor, the CNTs are able to penetrate through the HKUST-1 after the in situ growth of the crystals, which is verified by the observation of CNTs stretching out from the fracture surface of a cracked HKUST-1 crystal as shown in Figure 1 c. The CNT penetration strings the HKUST-1 crystals together for improved connection among crystals as well as that between crystals and the external CNT network, contributing to a robust and self-standing hybrid thin film. The as-prepared HKUST-1/CNT thin film was subsequently pyrolyzed at 800 °C for 3 h to yield the ISCF thin film. The complete carbonization of the HKUST-1/CNT thin film is confirmed by thermogravimetric analysis (TGA) and FTIR, owing to the constant weight and the absence of organic functional groups after pyrolysis, respectively (Supporting Information, Figure S2).[27,28] A subsequent nitric acid treatment was performed to remove the Cu species converted from the Cu metal sites in the HKUST-1 precursor. The removal of Cu and Cu_2O is confirmed by the complete absence of Cu-related peaks after acid treatment in the X-ray photoelectron spectroscopy (XPS) and x-ray diffraction (XRD) results. The absence of Cu and Cu_2O particles in the SEM image of the thin film after acid treatment also supports this result (Figure S3 c,d). It should be noted that through the acid treatment, the nanoscale Cu and Cu_2O particles serve as the templates to produce more meso-/macropores for ISCF film. The enriched meso-/macroporosity offers the carbon thin film with a greater potential for higher sulfur loading and improved electrolyte accessibility.

Figure 1 d shows the well retained self-standing and laminated structure of the obtained ISCF film (or ISCF-10/1) with a thickness of circa 20 μm, which is similar to that of the HKUST-1/CNT thin film. The octahedral morphology of the HKUST-1 crystal is also well preserved after carbonization (Figure 1 e,f). The CNTs stretching out from the porous carbon polyhedrons and intertwining with the external CNT network can be clearly observed in Figure 1 f, confirming the CNT interpenetration in the obtained ISCF. The interpenetration is also evidenced by the distinct observation of CNTs extending from the interior of the porous carbon polyhedron and connecting with the adjacent ones (Figure 1 g,h). The interpenetration construction endows the ISCF with fully connected conductive network, enriched active interfaces, and robust mechanical properties, holding great potential for efficient sulfur electrochemistry. The high I_G/I_D values in the Raman spectra (Figure 2 a) of the ISCF

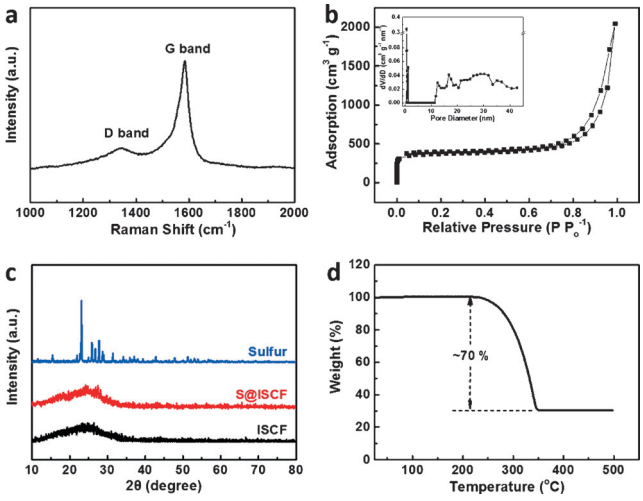

Figure 2. a) Raman spectra, b) N_2 adsorption–desorption isotherm and pore distribution (inset) of ISCF film. c) The XRD pattern of pure sulfur, ISCF, and S@ISCF composite. d) The TGA curve of S@ISCF in N_2 atmosphere with a heating rate of 5 °C min^{-1}.

indicate its highly graphitic properties and great capability to provide fast electron transfer for sulfur electrochemistry. The N_2 adsorption/desorption isotherm and the pore-size distribution (Figure 2b and the inset, respectively) reveals the hierarchical porosity of the ISCF owing to the abundance of micro-, meso-, and macropores. The ISCF delivers a high specific surface area (SSA, 1147.4 $m^2 g^{-1}$) and large pore volume (3.15 $cm^3 g^{-1}$), exerting a great structural superiority for high sulfur loading and uniform sulfur distribution.

The corresponding sulfur electrodes (S@ISCF) were prepared by using a melt-infusion process. The amorphous XRD pattern of S@ISCF electrode compared with those of CNTs and pure sulfur powder indicates the uniform sulfur distribution in the ISCF porous matrix (Figure 2c).[29,30] The sulfur content is around 70 wt% as determined by TGA as shown in Figure 2d. The S@ISCF electrode shows a thickness of approximately 20 μm and retains the self-standing and laminated structure as observed in the Supporting Information, Figure S4a. The TEM image and the corresponding elemental mapping reveal a uniform elemental distribution in the S@ISCF electrode (Figure S4b–d), strongly supporting the uniform distribution of sulfur in the ISCF matrix.

Galvanostatic charge–discharge tests were performed to evaluate the electrochemical performance of the S@ISCF electrode. The S@CNT and S@PCP electrodes based on pure CNTs and pure carbon polyhedrons, respectively were also tested for comparison. As shown in Figure 3a, all the electrodes show typical two-platform voltage curves, which is consistent with the two-stage sulfur electro-redox in an ether-based electrolyte.[31–33] Notably, the potential gap between the charge and discharge curves in the voltage profile of the S@ISCF electrode is much smaller than those of the S@CNT and S@PCP electrodes, while the cyclic voltammetry (CV) results (Figure 3b) consistently show much sharper peaks and smaller potential gaps between redox peaks for the S@ISCF electrode. These results indicate the remarkably improved electrochemical kinetics in the S@ISCF electrode, which is further confirmed by the smallest impedance before and after cycling in the EIS analysis (Supporting Information, Figure S5). Figure 3c shows the cycling performances of different electrodes with a controlled sulfur loading of 2.0 mg cm^{-2} at C/5 rate (1 C = 1675 mA g^{-1}). The S@ISCF electrode delivers the highest initial capacity of 1290.9 mAh g^{-1} and capacity retention of 960 mAh g^{-1} after 50 cycles. In contrast, the S@CNT and S@PCP electrodes exhibit much lower initial capacities (947.1 and 999.5 mAh g^{-1}, respectively) and capacities after 50 cycles (483.1 and 634.8 mAh g^{-1}, respectively).

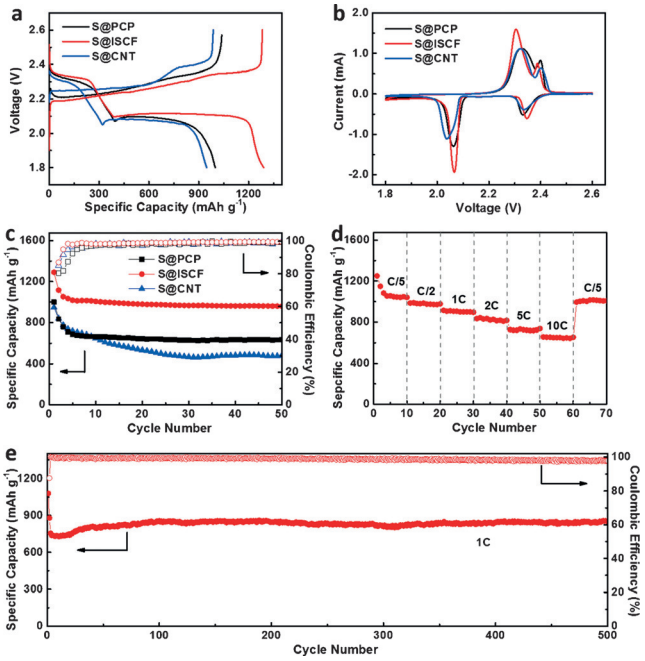

Figure 3. a) Voltage profiles, b) CV curves, and c) cycling performance comparisons among S@ISCF, S@PCP, and S@CNT electrodes. d) Rate response up to 10C and e) long-term cycling performance over 500 cycles at 1C rate of S@ISCF electrode.

The superior cycling performance of the S@ISCF electrode is attributed to its structural superiority stemming from the synergetic coupling of CNTs and the porous carbon polyhedrons. On the one hand, the high porosity of carbon polyhedrons overcomes the lack of SSA in CNTs to ensure uniform sulfur distribution, abundant active interfaces, and strong sulfur confinement. On the other hand, the CNT interpenetration not only improves the electrode conductivity by offering a fully connected conductive framework but also enriches the inner space of the pores for improved sulfur utilization. Moreover, the CNTs also interweave the electrode into a self-standing pliable thin film to buffer the volume variation during the cycling, avoiding the use of a nonconductive binder and further enhancing the conductivity of the electrodes. This functional integration of carbon polyhedrons and CNTs contribute to the reduced electrochemical impedance, enhanced sulfur utilization, and improved cycling stability for the S@ISCF electrode. Given the different functionality of the two components, ISCFs derived from precursors with different HKUST-1-to-CNT weight ratios, ISCF-5/1 and ISCF-20/1, were also prepared to investigate the influence of component ratio on cell performance. As shown in the Supporting Information, Figure S6, the S@ISCF electrode with a ratio of 10:1 delivers the optimum combination of CNTs and carbon polyhedrons by showing the minimum electrochemical polarization and the best cycling performance among the electrodes with different component ratios. This is ascribed to its optimal pore structure with both the highest SSA and largest pore volume compared to those of the others as shown in Table S1.

On the basis of these results, multi-rate and long-term cycling of the S@ISCF electrode were further performed to examine its rate capability and cyclability (Figure 3d,e). The S@ISCF electrode achieves a highly reversible capacity of 650 mAh g^{-1} at a high rate even up to 10C and recovers to around 1000 mAh g^{-1} when switched back to C/5, revealing its fast reaction kinetics and excellent electrode integrity. Moreover, the S@ISCF electrode exhibits outstanding cycling stability with a negligible capacity fading rate of 0.0054% per cycle after the second cycle and a coulombic efficiency consistently above 98% over 500 cycles under a rate of 1C. It should be pointed out that the rate and cycling performance of S@ISCF are much superior than those of the recently

reported sulfur electrodes based on MOFs-derived carbon hosts (Supporting Information, Table S2).

To achieve higher energy density in consideration of the requirements for scale-up commercialization, S@ISCF electrodes with higher areal sulfur loadings of 3.8, 6.4, and 8.0 mg cm^{-2} were also prepared by simply increasing the thickness of the electrodes to 36, 62, and 79 μm, respectively. The electrodes with higher sulfur loading exhibit high areal capacities up to 6.23 mAh g^{-1} over 50 cycles, surpassing that of the commercial Li-ion batteries (Figure 4a),[34,35] though

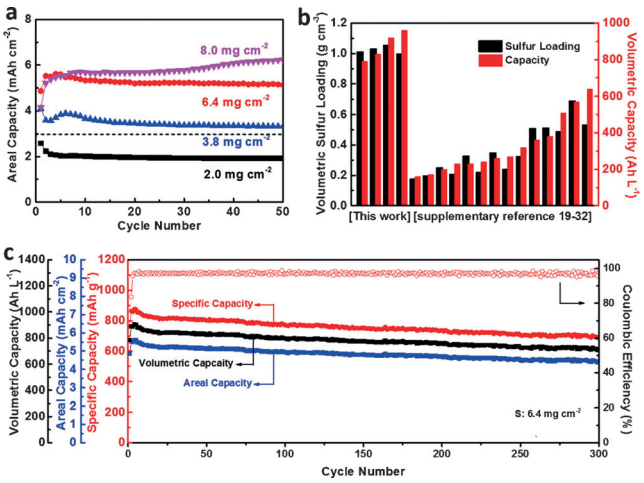

Figure 4. a) Areal capacities of S@ISCF electrodes with different sulfur loadings. b) Comparison of volumetric sulfur loading and capacity between S@ISCF and representative high sulfur loaded electrodes (see details in Table S3). c) Prolonged cycling performance of S@ISCF electrode with a high sulfur loading of 6.4 mg cm^{-2} at C/5 rate, and the corresponding areal and volumetric capacities.

a relatively limited capacity increment is observed when sulfur loading is further increased to 8.0 mg cm^{-2} owing to the impeded electron/ion transfer. Accordingly, the S@ISCF electrodes deliver high volumetric sulfur loading around 1.0 g cm^{-3} and volumetric capacity up to 960 Ah L^{-1}, representing the best performance among the recently reported high-sulfur-loading electrodes (Figure 4b and the Supporting Information, Table S3). Excellent cyclability was also achieved for the S@ISCF electrode with a high sulfur loading of 6.4 mg cm^{-2} over 300 cycles at C/5 rate (Figure 4c) with reversible high areal capacity and volumetric capacity. The great capability for sulfur loading and satisfactory sulfur electrochemistry of the S@ISCF electrode are due to the abundant active interfaces, strong sulfur confinement, robust electrode integrity, and long-range conductivity provided by the unique hybridization of CNTs and MOF-derived carbon polyhedrons. These results strongly demonstrate the competitive potential of this cathode structural design for practical applications.

In summary, we developed a self-standing, interpenetrated conductive framework through a rational hybridization of CNTs and MOF-derived carbon polyhedrons as the cathode host for Li–S batteries. The intertwined CNT endows the electrodes with superior long-range conductivity and favorable structural integrity, while the strung carbon polyhedrons ensure sufficient active interfaces and efficient sulfur confinement. Importantly, the CNT penetration greatly enriches the pore space in the carbon polyhedrons and enables higher sulfur utilization. Attributed to the synergetic combination of CNTs and carbon polyhedrons, outstanding cyclability with an ultra-low capacity decay of 0.0054% per cycle over 500 cycles, excellent rate capability up to 10 C, and an ultra-high volumetric capacity of 960 Ah L^{-1} were achieved for the corresponding electrodes. This work offers a facile and customized strategy to achieve advanced sulfur cathodes with high energy density, which could promote the commercialization and practical application of Li–S batteries.

Acknowledgements

This work was supported by the National Key Research and Development Program of China (2016YFA0200204), National Basic Research Program of China 973 Program (2015CB655302), and the National Natural Science Foundations of China (NSFC 21671171). This research was also supported by the Natural Sciences and Engineering Research Council of Canada (NSERC) through grants to Z.C. and the University of Waterloo.

Conflict of interest

The authors declare no conflict of interest.

Keywords: carbon nanotubes · energy storage · high energy density · lithium–sulfur batteries · metal–organic frameworks

How to cite: *Angew. Chem. Int. Ed.* **2017**, *56*, 6176–6180
Angew. Chem. **2017**, *129*, 6272–6276

[1] A. Manthiram, Y. Fu, S. H. Chung, C. Zu, Y. S. Su, *Chem. Rev.* **2014**, *114*, 11751–11787.
[2] P. G. Bruce, S. A. Freunberger, L. J. Hardwick, J. M. Tarascon, *Nat. Mater.* **2012**, *11*, 19–29.
[3] J. Xiao, *Adv. Energy Mater.* **2015**, *5*, 1501102.
[4] Y. X. Yin, S. Xin, Y. G. Guo, L. J. Wan, *Angew. Chem. Int. Ed.* **2013**, *52*, 13186–13200; *Angew. Chem.* **2013**, *125*, 13426–13441.
[5] R. Xu, J. Lu, K. Amine, *Adv. Energy Mater.* **2015**, *5*, 1500408.
[6] G. R. Li, M. Ling, Y. F. Ye, Z. P. Li, J. H. Guo, Y. F. Yao, J. F. Zhu, Z. Lin, S. Q. Zhang, *Adv. Energy Mater.* **2015**, *5*, 1500878.
[7] H. L. Pan, X. L. Wei, W. A. Henderson, Y. Y. Shao, J. Z. Chen, P. Bhattacharya, J. Xiao, J. Liu, *Adv. Energy Mater.* **2015**, *5*, 1500113.
[8] K. T. Lee, R. Black, T. Yim, X. L. Ji, L. F. Nazar, *Adv. Energy Mater.* **2012**, *2*, 1490–1496.
[9] W. D. Zhou, X. C. Xiao, M. Cai, L. Yang, *Nano Lett.* **2014**, *14*, 5250–5256.
[10] Y. Son, J. S. Lee, Y. Son, J. H. Jang, J. Cho, *Adv. Energy Mater.* **2015**, *5*, 1500110.
[11] G. R. Li, C. Wang, W. L. Cai, Z. Lin, Z. P. Li, S. Q. Zhang, *NPG Asia Mater.* **2016**, *8*, e317.
[12] X. L. Wang, G. Li, J. D. Li, Y. N. Zhang, A. Wook, A. P. Yu, Z. W. Chen, *Energy Environ. Sci.* **2016**, *9*, 2533–2538.
[13] Y. Yang, G. Zheng, Y. Cui, *Chem. Soc. Rev.* **2013**, *42*, 3018–3032.

[14] J. X. Song, M. L. Gordin, T. Xu, S. R. Chen, Z. X. Yu, H. Sohn, J. Lu, Y. Ren, Y. H. Duan, D. H. Wang, *Angew. Chem. Int. Ed.* **2015**, *54*, 4325 – 4329; *Angew. Chem.* **2015**, *127*, 4399 – 4403.
[15] W. D. Zhou, C. M. Wang, Q. L. Zhang, H. D. Abruna, Y. He, J. W. Wang, S. X. Mao, X. C. Xiao, *Adv. Energy Mater.* **2015**, *5*, 1401752.
[16] M. Li, Y. N. Zhang, X. L. Wang, W. Ahn, G. P. Jiang, K. Feng, G. Lui, Z. W. Chen, *Adv. Funct. Mater.* **2016**, *26*, 8408 – 8417.
[17] W. Xia, A. Mahmood, R. Q. Zou, Q. Xu, *Energy Environ. Sci.* **2015**, *8*, 1837 – 1866.
[18] X. W. Liu, T. J. Sun, J. L. Hu, S. D. Wang, *J. Mater. Chem. A* **2016**, *4*, 3584 – 3616.
[19] Z. Q. Li, C. X. Li, X. L. Ge, J. Y. Ma, Z. W. Zhang, Q. Li, C. X. Wang, L. W. Yin, *Nano Energy* **2016**, *23*, 15 – 26.
[20] F. X. Wu, E. B. Zhao, D. Gordon, Y. R. Xiao, C. C. Hu, G. Yushin, *Adv. Mater.* **2016**, *28*, 6365 – 6371.
[21] Z. Yuan, H. J. Peng, J. Q. Huang, X. Y. Liu, D. W. Wang, X. B. Cheng, Q. Zhang, *Adv. Funct. Mater.* **2014**, *24*, 6105 – 6112.
[22] Q. Sun, X. Fang, W. Weng, J. Deng, P. N. Chen, J. Ren, G. Z. Guan, M. Wang, H. S. Peng, *Angew. Chem. Int. Ed.* **2015**, *54*, 10539 – 10544; *Angew. Chem.* **2015**, *127*, 10685 – 10690.
[23] R. H. Baughman, A. A. Zakhidov, W. A. de Heer, *Science* **2002**, *297*, 787 – 792.
[24] Z. Q. Lin, Z. P. Zeng, X. C. Gui, Z. K. Tang, M. C. Zou, A. Y. Cao, *Adv. Energy Mater.* **2016**, *6*, 1600554.
[25] Y. Y. Mao, J. W. Li, W. Cao, Y. L. Ying, P. Hu, Y. Liu, L. W. Sun, H. T. Wang, C. H. Jin, X. S. Peng, *Nat. Commun.* **2014**, *5*, 5532.
[26] Y. H. Luo, J. G. Huang, J. A. Jin, X. S. Peng, W. Schmitt, I. Ichinose, *Chem. Mater.* **2006**, *18*, 1795 – 1802.
[27] K. Okada, R. Ricco, Y. Tokudome, M. J. Styles, A. J. Hill, M. Takahashi, P. Falcaro, *Adv. Funct. Mater.* **2014**, *24*, 1969 – 1977.
[28] T. Toyao, K. Liang, K. Okada, R. Ricco, M. J. Styles, Y. Tokudome, Y. Horiuchi, A. J. Hill, M. Takahashi, M. Matsuoka, P. Falcaro, *Inorg. Chem. Front.* **2015**, *2*, 434 – 441.
[29] C. F. Zhang, H. B. Wu, C. Z. Yuan, Z. P. Guo, X. W. Lou, *Angew. Chem. Int. Ed.* **2012**, *51*, 9592 – 9595; *Angew. Chem.* **2012**, *124*, 9730 – 9733.
[30] X. L. Ji, K. T. Lee, L. F. Nazar, *Nat. Mater.* **2009**, *8*, 500 – 506.
[31] S. Zhang, K. Ueno, K. Dokko, M. Watanabe, *Adv. Energy Mater.* **2015**, *5*, 1500117.
[32] M. Barghamadi, A. S. Best, A. I. Bhatt, A. F. Hollenkamp, M. Musameh, R. J. Rees, T. Rüther, *Energy Environ. Sci.* **2014**, *7*, 3902 – 3920.
[33] J. T. Yeon, J. Y. Jang, J. G. Han, J. Cho, K. T. Lee, N. S. Choi, *J. Electrochem. Soc.* **2012**, *159*, A1308 – A1314.
[34] M. S. Whittingham, *Chem. Rev.* **2004**, *104*, 4271 – 4301.
[35] L. X. Miao, W. K. Wang, K. G. Yuan, Y. S. Yang, A. B. Wang, *Chem. Commun.* **2014**, *50*, 13231 – 13234.

Manuscript received: January 19, 2017
Revised: February 23, 2017
Final Article published: March 22, 2017

